Sensors and Actuators B 162 (2012) 135–142

Contents lists available at SciVerse ScienceDirect

Sensors and Actuators B: Chemical

journal homepage: www.elsevier.com/locate/snb

Morphology-controllable gold nanostructures on phosphorus doped diamond-like carbon surfaces and their electrocatalysis for glucose oxidation

Aiping Liu[a,b,*], Qinghua Ren[a], Tao Xu[a], Ming Yuan[a], Weihua Tang[c]

[a] Center for Optoelectronics Materials and Devices, Key Laboratory of Advanced Textile Materials and Manufacturing Technology, Ministry of Education, Zhejiang Sci-Tech University, Hangzhou 310018, China
[b] State Key Lab of Silicon Materials, Zhejiang University, Hangzhou 310027, China
[c] State Key Laboratory of Information Photonics and Optical Communication, Beijing University Posts and Telecommunications, Beijing 100876, China

ARTICLE INFO

Article history:
Received 28 October 2011
Received in revised form
11 December 2011
Accepted 16 December 2011
Available online 24 December 2011

Keywords:
Morphology-controllable gold nanostructures
Diamond-like carbon
Glucose oxidation
Non-enzymatic biosensor

ABSTRACT

Gold nanostructures with controllable morphologies were synthesized by electrochemical deposition on phosphorus doped diamond-like carbon (DLC:P) film surfaces. The morphology of the as-synthesized gold nanostructures controlled by deposition potentials affected the electrocatalytic behavior of Au/DLC:P electrodes. The gold nanostructures obtained at −0.1 V showed a 3D flower-like morphology (consisting of staggered nanosheets), and exhibited higher electrocatalytic activity towards glucose electrooxidation at the potential below 0.1 V in alkaline media compared with other gold nanostructures (hemispherical and branched clusters) in terms of more unsaturated gold (2 2 0) and (3 1 1) crystal faces and monolayer oxide mediators on gold surfaces. The gold nanostructures with controllable morphologies were hence promising for the development of an electrocatalyst of non-enzymatic glucose sensor.

1. Introduction

Diabetes is one of the most serious diseases, which is characterized by an abnormal level of blood glucose due to the defects in insulin production and insulin action [1]. Electrochemical glucose sensor has been extensively investigated due to its important applications in clinical diagnosis of diabetes, food analysis and glucose fuel cells [2,3]. The sensitivity and stability of glucose sensors depend on the physicochemical characteristics of electrode materials employed as a transducer and catalytic activity of redox mediators. Metallic nanostructured materials with high electrocatalytic activities have been widely developed by various synthetic methods [4–6] and used to oxidize carbohydrates in the aqueous solution [7–10]. The nanostructured gold, considering its potential in catalysts, electronic detectors, optical devices, electrochemical sensors or biosensors [4,6,11–13], has been particularly given great attention and investigation due to its controllable electronic and optical properties, great promotion for the direct electron transfer, and anti-poisoning ability for adsorbed intermediates. The chemical compositions, sizes, shapes and distribution of gold nanostructures, which play crucial roles in their electrocatalytic properties, can be successfully tailored and controlled by wet-chemical methods or colloid chemistry [13–20] when using templates or precursors or matrix, such as porous materials [21], geranium leaves [15], polypyrrole or polyelectrolyte modified substrate [22,23], as well as polystyrene spheres [24] to inherit a certain morphology from their previous templates or precursors. However, the dosages of surfactants or organic additives, reaction rate and temperature need be accurately controlled in these chemical methods and the resulted metallic nanostructures must be separated and recycled to remove heterogeneous impurities or templates before immobilized to a solid substrate [25]. A substitutable simple, rapid and direct method to produce well-defined metal nanostructures on a certain substrate is electrochemical deposition, which is a versatile technique used to synthesize desirable nanostructures for various applications [22,24,26–29]. The shapes, sizes and coverage of electrodeposited gold nanostructures can be elaborately controlled by simply changing reactant concentration, reaction time and deposition potentials in the reaction process [22,27]. For example, Wang et al. electrochemically synthesized diameter-controlled hierarchical flower-like gold microstructures by changing the deposition time and potential [27]. Li and Shi fabricated two-dimensional gold nanoparticles with dendritic, sheet, flower-like and pinecone-like structures by electrochemical deposition onto indium tin oxide glass substrate modified with thin polypyrrole film and controlled their catalytic activity on electrochemical reduction of oxygen [22].

* Corresponding author at: Center for Optoelectronics Materials and Devices, Key Laboratory of Advanced Textile Materials and Manufacturing Technology, Ministry of Education, Zhejiang Sci-Tech University, Hangzhou 310018, China.
Tel.: +86 571 86843468; fax: +86 571 86843222.
E-mail address: liuaiping1979@gmail.com (A. Liu).

0925-4005/$ – see front matter © 2011 Elsevier B.V. All rights reserved.
doi:10.1016/j.snb.2011.12.050

Furthermore, the substrate material should be well-chosen to provide desirable electrical connection to the metallic nanoparticles on it. Carbon materials, including glassy carbon, pyrolytic graphite, carbon nanotube, diamond and diamond-like carbon (or amorphous carbon), are regarded as ideal electrode materials due to their wide potential range, low residual current, reproducible surface structure and suitability for chemical modification [30–34]. Glucose detection using different carbon electrodes has been broadly reported in the past few years [7,8,30,33–35]. Among these carbon materials, doped DLC or amorphous carbon film with attractive features [36], such as room temperature preparation, reasonable conductivity, wide potential window, low background current, chemical stability and biocompatibility represents a favorable substrate electrode for metallic nanoparticles anchoring and can be used as an electrochemical sensor [33,37–41]. However, to the best of our knowledge, there were few reports on glucose oxidation at morphology-controllable gold nanostructures modified conductive DLC electrodes. Herein, we report the direct formation of gold nanostructures with different morphologies in situ on the phosphorus doped DLC (DLC:P) thin film electrodes by a simple and efficient electrodeposited approach. The morphology of gold nanostructures can be solely controlled by changing deposition potentials during preparation. The gold particles with pseudo-spherical, dendritic or branched and flower-like (consisting of staggered nanosheets) nanostructures are generated. Furthermore, the electrocatalytic activity for glucose oxidation and surface properties of these gold nanostructures depend strongly on their morphologies.

2. Experimental

2.1. Reagents

$HAuCl_4 \cdot 3H_2O$ (purity 99.99%) and D-Glucose (purity 98%) were supplied by Sigma, USA. All other chemicals were of analytical grade and used without further purification. The water was obtained from a Millipore Q purification system (resistivity >18 MΩ cm).

2.2. Preparation of DLC:P electrodes anchored with gold nanostructures

The DLC:P thin films were deposited on conductive p-Si (1 0 0) substrates (0.001–0.0035 Ω cm) by a filtered cathodic vacuum arc deposition system (Nanofilms) using the same procedure described in literature [38,39]. Briefly, when the pressure of vacuum chamber was down to 2×10^{-6} Torr, 15-sccm PH_3 (99.999%) was continuously introduced into the vacuum chamber to maintain a dynamically balanced chamber pressure. DLC:P films with a thickness about 90 nm were deposited on the silicon substrate under a fixed negative pulse voltage of 500 V. The as-prepared DLC:P films were pretreated in a 0.1 M NaOH solution as described in literature [33]. The NaOH-treated DLC:P films were then immersed into a 0.1 M H_2SO_4 solution containing 0.5 mM $HAuCl_4$ to electrodeposit gold nanoparticles on the film surfaces. An electrochemical workstation (CHI 660C, USA) with a three-electrode system including DLC:P working electrode, Ag/AgCl (saturated KCl) reference electrode and platinum foil counter electrode, was used. The deoxygenated electrolytes were prepared by bubbling the electrolytes with dry N_2 for 30 min before experiment. The deposition potential step was controlled from 0.9 to 0.5 V, 0.2 V and −0.1 V (vs. Ag/AgCl), respectively, with a potential pulse width of 100 s and sampling interval of 0.002 s. The prepared Au/DLC:P samples were correspondingly labeled as Au/DLC:P-0.5, Au/DLC:P-0.2 and Au/DLC:P-0.1, respectively. The as-prepared Au/DLC:P electrodes were cycled in a 0.1 M H_2SO_4 solution until stable voltammograms were achieved, indicating the complete cleaning of the gold active areas. The real surface areas of gold loading were estimated using the same procedure described in literature [38].

2.3. Characterization and measurements

The compositions of DLC:P films were measured by X-ray photoemission spectroscopy (XPS, PHI ESCA 5700) with Al K_α (1486.6 eV) as the X-ray source and quantified as 4.3, 90.6 and 5.1 at.% for phosphorus, carbon and oxygen elements, respectively, corresponding to the P 2p, C 1s and O 1s core level spectra. The morphologies of gold nanostructures were observed by transmission electron microscopy (TEM, Philips CM 300 FEG) at 200 kV and scanning electron microscopy (SEM, Hitachi S4800) equipped with an energy-dispersive X-ray spectroscopy (EDS). The X-ray diffraction (XRD) patterns of the gold nanostructures were recorded by a diffractometer (Bruker AXS D8) with an area detector operating under a voltage of 40 kV and a current of 40 mA using Cu K_α radiation (λ = 0.15418 nm).

The electrochemical properties of glucose oxidation at Au/DLC:P electrodes with different gold nanostructures were investigated in a 0.1 M NaOH solutions using the above three-electrode system. The interference experiment was carried out by recording a steady-state current–time curve under an optimal potential with a stirring rate of 300 rpm. All electrochemical experiments were carried out at 20 °C monitored by a thermostatic water jacket.

3. Results and discussion

3.1. Microstructures of gold with controllable morphologies

Fig. 1 shows different magnifications of SEM images of gold nanostructures electrodeposited on DLC:P surfaces at adjusted potential steps. At the higher deposition potential of 0.5 V, the as-deposited gold shows a 3D pseudo-spherical nanostructure (Fig. 1a and b) with a medial diameter about 126 nm (Fig. 2a). When the deposition potential decreases to 0.2 V, gold morphology changes to dendritic or branched structure composed of many nanoparticles, as shown in Fig. 1c and d. Further decreasing the potential to −0.1 V, we obtain a flower-like (consisting of staggered nanosheets) nanostructure (Fig. 1e and f) with a medial diameter about 135 nm (Fig. 2a). Local magnification reveals that the 2D nanoflakes are about 20–40 nm in thickness (Fig. 1f). At the lower deposition potential, the particle sizes are more inhomogenous. This is possibly due to a higher overpotential providing more active positions for nucleation and growth of gold. The EDX spectrum of Au/DLC:P sample (Fig. 2b) confirms the existence of gold.

It is generally believed that the crystal morphology is related to the formation condition away from the thermodynamic equilibrium [42,43], which is determined by the overpotential in electrochemical deposition [26]. Under the higher deposition potential (0.5 V), the gold nanostructure is formed when close to the thermodynamic equilibrium. The crystal has a slower growth rate and the morphology turns to be spherical to maintain a minimum surface energy (Fig. 1a and b). According to the lowest-energy principle, the growth rate along the closely packed (1 1 1) plane is obviously enhanced due to the lowest surface energy of (1 1 1) crystalline face [44], leading to the formation of hemispherical nanostructure with preferential growth direction along [1 1 1], as confirmed by the corresponding XRD pattern (Fig. 3a). Under a lower deposition potential (0.2 V), the gold nanostructure is formed farer away from the thermodynamic equilibrium, which provides the crystal a relatively higher growth rate and a thermodynamically stable branched structure. At the lowest deposition potential of −0.1 V, the potential is much more negative than the standard

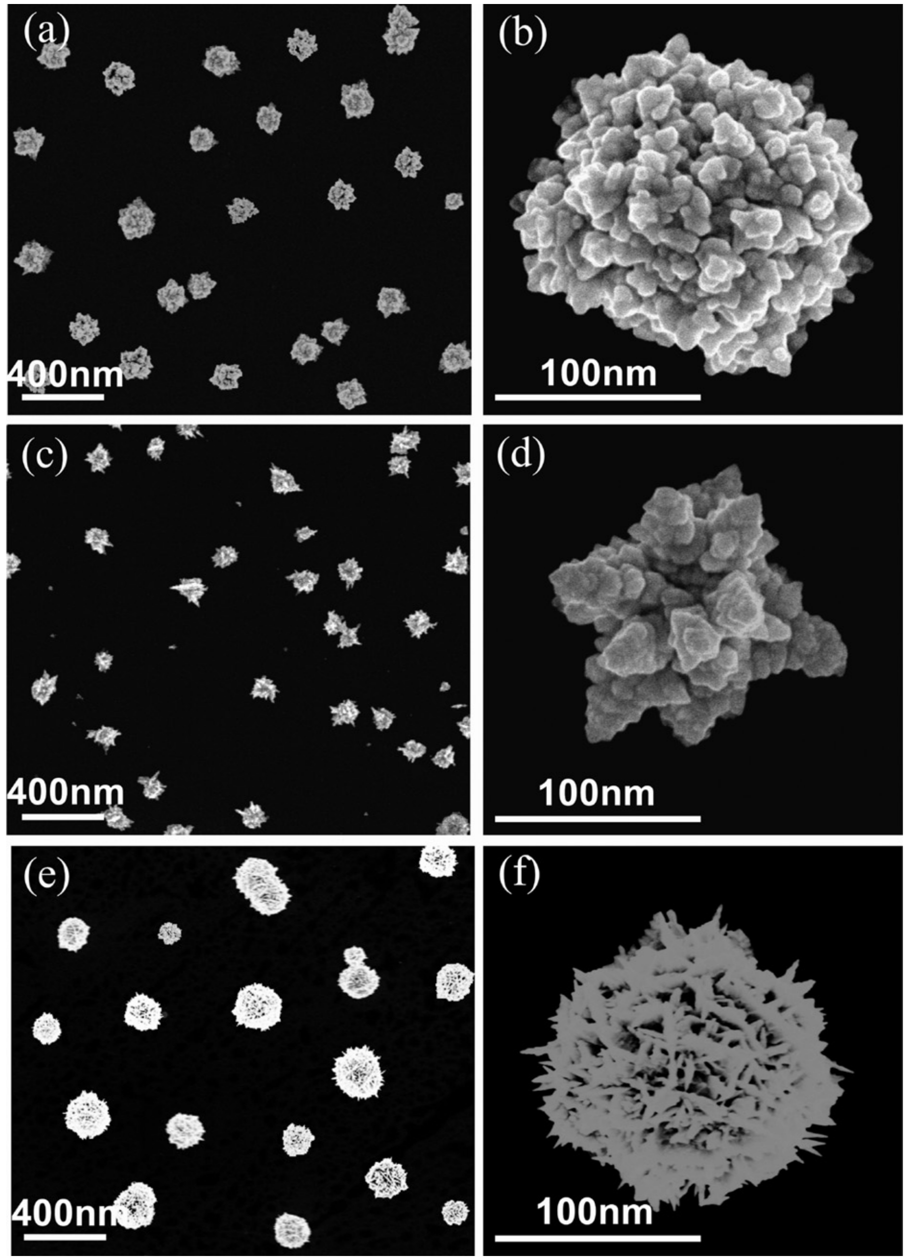

Fig. 1. Low magnification (a, c, and e) and high magnification (b, d, and f) scanning electron microscope images of gold nanostructures synthesized by electrochemical deposition. (a) and (b) hemispherical accumulation deposited at 0.5 V, (c) and (d) branched clusters deposited at 0.2 V, (e) and (f) flower-like nanostructures (consisting of staggered nanosheets) deposited at −0.1 V.

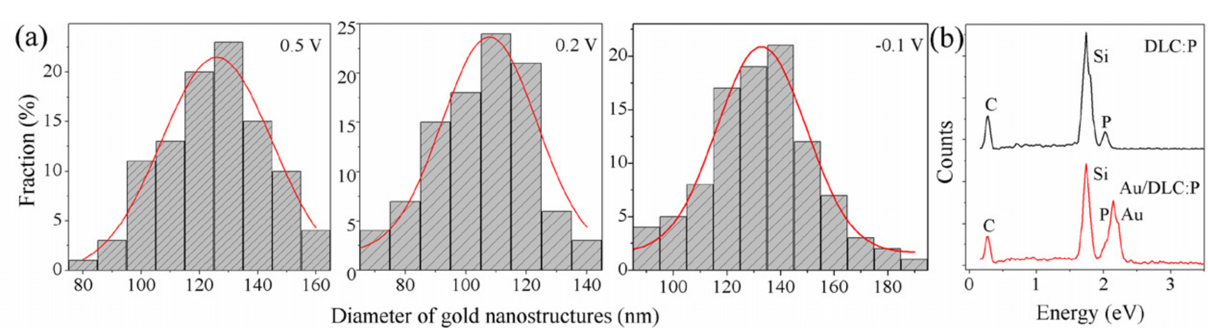

Fig. 2. (a) Diameter distribution of gold nanostructures with controllable morphologies prepared under different electrochemical deposition potentials, and (b) EDX spectra of Au/DLC:P and DLC:P surfaces.

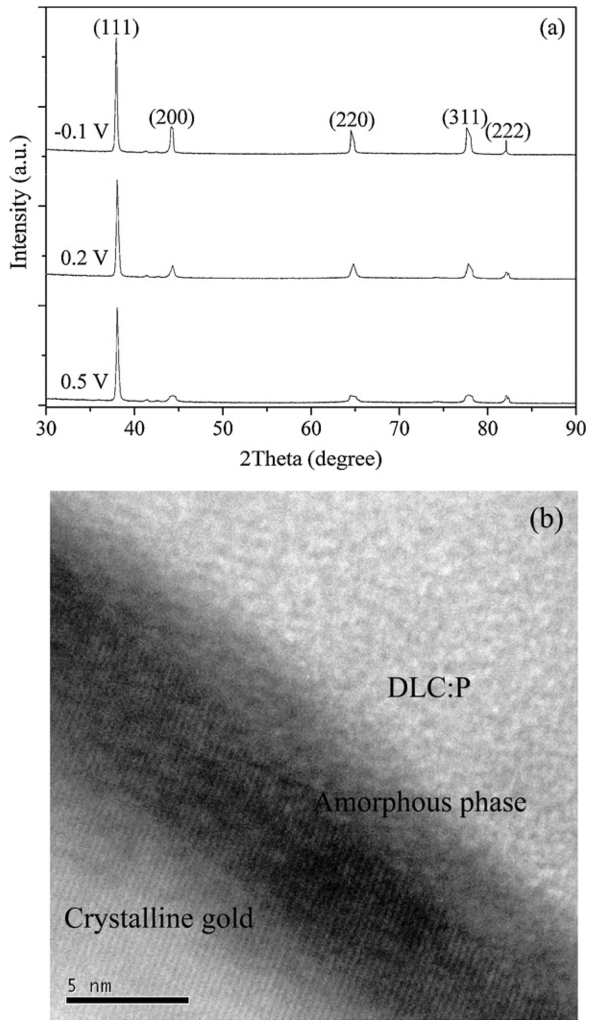

Fig. 3. (a) X-ray diffraction patterns of gold nanostructures with controllable morphologies, and (b) high-resolution TEM image at the interface area of gold nanostructure and DLC:P film.

electrode potential of gold, resulting in a highest growth rate of the crystals and a maximal surface energy. The XRD pattern of Au/DLC:P-0.1 indicates five obvious peaks at about $2\theta = 38.0$, 44.3, 64.5, 77.6 and 81.8° which are assigned to the (1 1 1), (2 0 0), (2 2 0), (3 1 1) and (2 2 2) diffraction peaks of metallic gold, respectively [14]. The intensity ratio between the (2 0 0) and (1 1 1) diffraction peaks is much lower than the standard file (JCPDS, 0.33) [45]. Therefore, our gold nanostructures are primarily dominated by (1 1 1) facets, namely their (1 1 1) planes tend to be preferentially oriented parallel to the surface of the supporting substrate [27,46]. With the Scherrer equation [47], the grain size of gold is calculated to be about 20 nm from the full width at half maximum. The interface between gold nanostructure and DLC:P film is further characterized by TEM. Fig. 3b exhibits clear lattice planes, showing a perfect single-crystal structure of gold.

3.2. Deposition mechanism of gold

Fig. 4 displays the cyclic voltammograms of Au/DLC:P electrodes in a 0.1 M H_2SO_4 at $0.1\,V\,s^{-1}$. The reduction and oxidation peaks related to Au can be observed at about 0.75 V in the negative scan and 1.20 V on the positive scan, respectively. The obvious cathodic peak at ca. −0.28 V might be attributed to the reduction of recalcitrant oxides formed on the nanostructured gold in the positive sweep, as observed by Burke [48]. The surface areas of gold

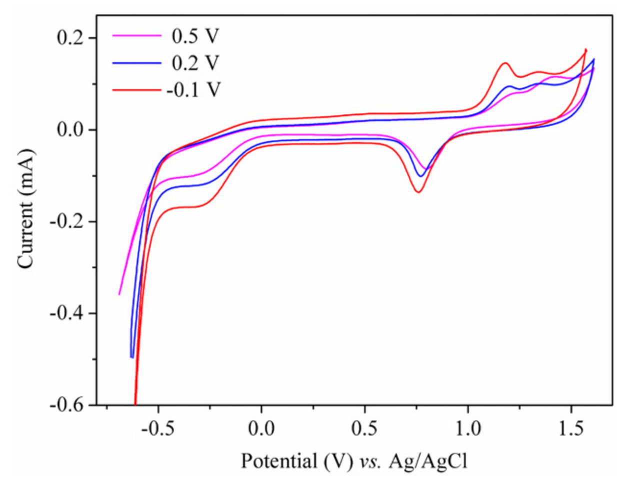

Fig. 4. Cycle voltammograms of Au/DLC:P electrodes in a 0.1 M H_2SO_4 solution at $0.1\,V\,s^{-1}$.

nanostructures are estimated from the charge consumed in the reduction of the surface oxide monolayer of gold in the cathodic scan using H_2SO_4 as a probe, as described in literature [38]. The surface areas of gold loading are estimated to be 0.041, 0.053 and 0.078 cm^2 for Au/DLC:P-0.5, Au/DLC:P-0.2 and Au/DLC:P-0.1, respectively. The current densities of the DLC:P electrodes with different gold nanostructures are therefore used in this paper when currents divided by the surface area of gold nanostructures.

In order to investigate the nucleation process of gold nanostructures on the DLC:P surfaces, we collect the potentiostatic current–time curves (Fig. 5a) with potential step from 0.9 V to 0.5, 0.2 and −0.1 V, respectively. This chronoamperometric curve can be divided into four successive time intervals, namely the double-layer charging and initial nucleation process, the free growth of independent nuclei and formation of new nucleation sites without overlapping, the growth of independent nuclei and their overlap, and the overlapping of diffusion zones of different nuclei [49]. The $I^{1/2}$ vs. t plot is linear in the phase of independent nuclei growth and new nucleation formation, indicating a 3D-nucleation process with diffusion control [49]. According to Scharifker and Hills' viewpoint, there are two kinds of nucleation processes, instantaneous nucleation and progressive nucleation, for the diffusion-limited growth [50]. Our current–time curve is further compared with the two limiting mechanisms using the reduced variables I_m and t_m, as shown in Fig. 5b–d. Here t_m is the time corresponding to the maximum current I_m in the chronoamperometric curve. The experimental result agrees better with the progressive nucleation mechanism. Similar results had been obtained for platinum electrodeposition on diamond and pyrolytic graphite [51,52].

3.3. Electrocatalytic activities towards glucose oxidation

The morphology-controllable gold nanostructures exhibit obviously electrocatalytic activities towards glucose oxidation in alkaline media. The glucose oxidation occurs from about −0.5 V on Au/DLC:P-0.5 electrode and displays two oxidation peaks at −0.04 V (Peak A) and 0.32 V (Peak B), as shown in Fig. 6a. During the negative sweep, an intense re-oxidation peak of glucose at about 0.03 V (Peak C) appears in the same potential region as soon as the gold oxides are reduced. Increasing the concentration of glucose in the solution moves the three peaks to the positive direction. The linear detection range of glucose with the Au/DLC:P-0.5 electrode is identified from about 0.5 to 25 mM (covering blood glucose levels in diabetic patients) with a detection limit of 300 μM and a sensitivity of 37 μA/(cm^2 mol) for Peak A, 320 μM and 55 μA/(cm^2 mol) for

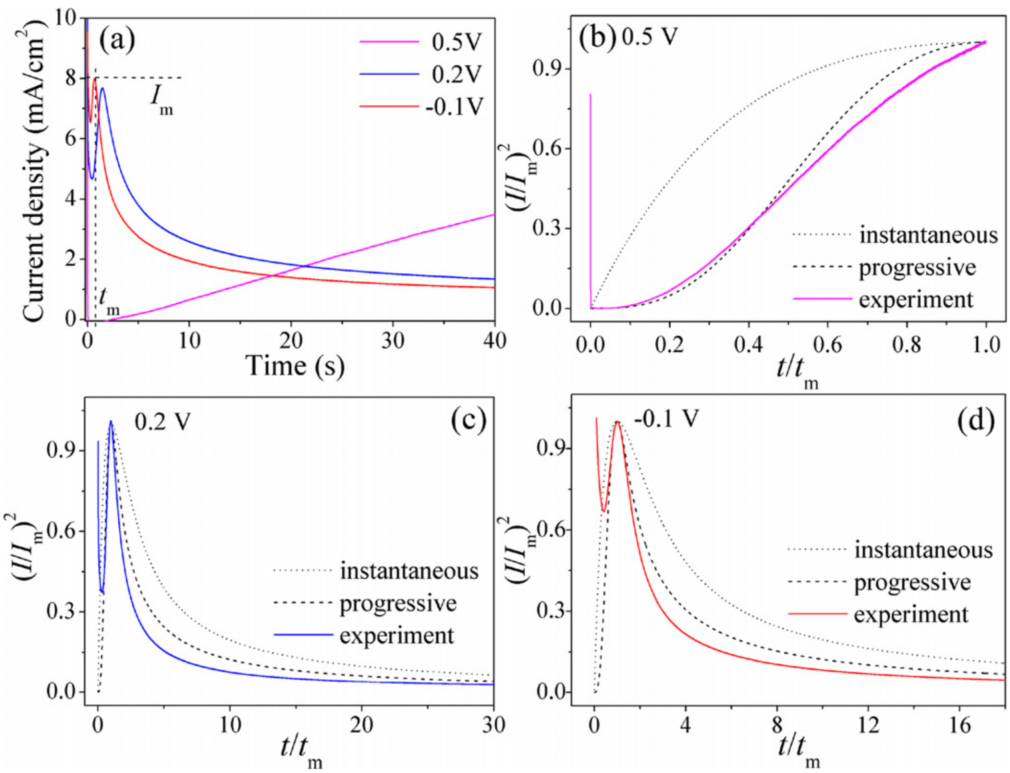

Fig. 5. (a) Potentiostatic current–time transients of gold deposits on DLC:P film surfaces under different deposition potentials, (b)–(d) current–time transient response plotted in reduced variables I/I_m vs. t/t_m for gold deposition on the DLC:P electrodes under different potential steps. The t_m is the time corresponding to the maximum current I_m under different deposition potentials in (a).

Peak B, and 880 μM and 10 μA/(cm^2 mol) for Peak C. For Au/DLC:P-0.2 electrode, the oxidation peak of glucose (Peak C) is more intense. The detection limit and sensitivity for glucose with this electrode is identified about 150 μM and 50 μA/(cm^2 mol) for Peak B and 500 μM and 95 μA/(cm^2 mol) for Peak C. The Au/DLC:P-0.1 electrode displays more arrestive electrocatalytic activities towards glucose oxidation. Three intense re-oxidation peaks of glucose can be detected during the negative sweep. The linear detection range of glucose with the Au/DLC:P-0.1 electrode is identified from about 0.3 to 30 mM with a detection limit of 150 μM and a sensitivity of 20 μA/(cm^2 mol) for Peak A, 1.8 mM and 100 μA/(cm^2 mol) for Peak C, 270 μM and 140 μA/(cm^2 mol) for Peak D, and 5 μM and 110 μA/(cm^2 mol) for Peak E. Though Au/DLC:P-0.1 electrode might have a wider linear detection range and higher sensitivity, the current response for Peak B is lower compared with those obtained at other two electrodes. This might be explained by the electrocatalysis model of hydrous oxide mediation of gold. It is known that gold adatoms at the gold electrode surface undergo pre-monolayer oxidation to form hydrous oxide species with highly reactive, including a cationic Au(I) species $[Au^+(H_2O)_n]_{ads}$ at a lower potential and anionic Au(III) hydrous oxide species $[Au_2(OH)_9{}^{3-}]_{ads}$ at a higher potential [53]. The oxidation of glucose in alkaline media is mainly mediated by the Au(III) hydrous oxide species at a higher potential (might be over 0.1 V in the present result) and a combination of Au(I) and Au(III) mediators at the potential below 0.1 V. The observed Peak A and Peak B at Au/DLC:P-0.5 electrode could be controlled by the increased Au(I) mediator and the Au(III) one, respectively. The first-order curves of the reaction rate are obtained according to the kinetic theory of mediator-catalyzed oxidation processes [54], as show in the inset of Fig. 6a. However, the increasing surface area of gold nanostructures results in a decrease of current response, even no enhancement for Peak B (Fig. 6b and c) in the positive sweep due to the over oxidation of gold active states (the increased oxidation and reduction peaks related to gold in Fig. 4). The gluconorate anion might be repulsed by the Au(III) mediator sites assumed to bear a similar anionic charge [53]. On the reverse sweep, the surface is inactive due to the glucose oxidation until the monolayer film of gold hydrous oxide is reduced below 0.1 V. The high rates of reaction for Peaks C–E on the negative sweep might be due to the regenerated Au(I) mediator after the reduction of Au(III) one by glucose. The electrostatic interaction between the cationic mediator $[Au^+(H_2O)_n]$ and the anionic form of glucose is evidently a major factor in promoting oxidation of glucose at the low potentials in the reverse sweep.

Furthermore, the electrocatalytic character is related to the crystal structures of the nanoarchitectures. It is clear from the XRD patterns that all samples have lines of gold (1 1 1) and (2 0 0) crystal faces. Furthermore, Au/DLC:P-0.1 sample with flower-like nanostructures shows the evident lines of gold (2 2 0) and (3 1 1) faces (Fig. 2a). The gold atoms in gold (2 2 0) and (3 1 1) crystal faces have higher unsaturation than those in gold (1 1 1) and (2 0 0) faces because of their high miller indexes exposing surface irregularities [55]. Thus, they can adsorb more glucose molecules easily and have relatively higher catalytic activity. Bhargava et al. also observed a significant increase in the response of glucose oxidation at the honeycomb nanogold networks with highly active sites and high surface energy (3 1 1) facets [56]. Thus, the surface characters of gold nanostructures including surface area, oxidation degree and crystal structures operate collectively the electrocatalytic reactions occurred on the surface of nanomaterials [56]. The present electrochemical method can be used to fabricate morphology-controllable gold nanostructures with adjustable electrochemical behaviors, which may further be applied as an electrocatalyst of non-enzymatic glucose sensor and elaborately investigate the oxidation process of glucose.

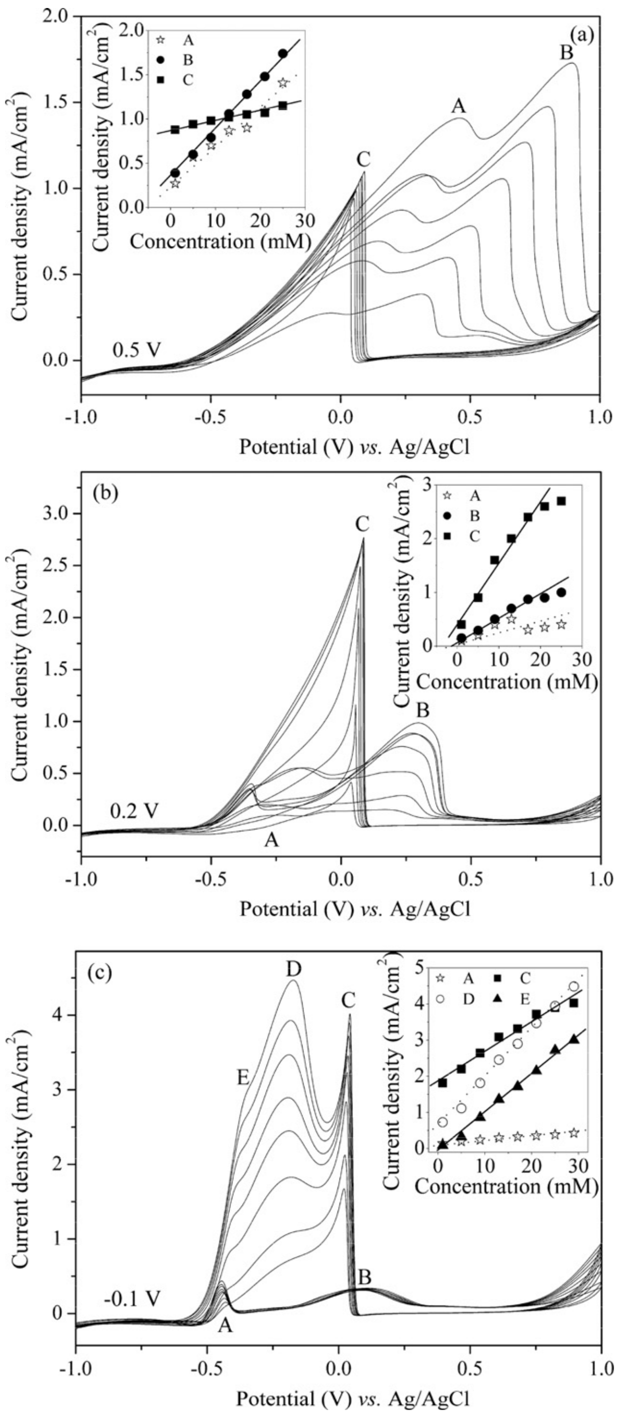

Fig. 6. Cycle voltammograms of glucose oxidation on the Au/DLC:P electrodes prepared under (a) 0.5 V, (b) 0.2 V, and (c) −0.1 V at 50 mV s^{-1} in a 0.1 M NaOH solution with continuous glucose injection. The insets show the linear relations between peak current densities and glucose concentrations.

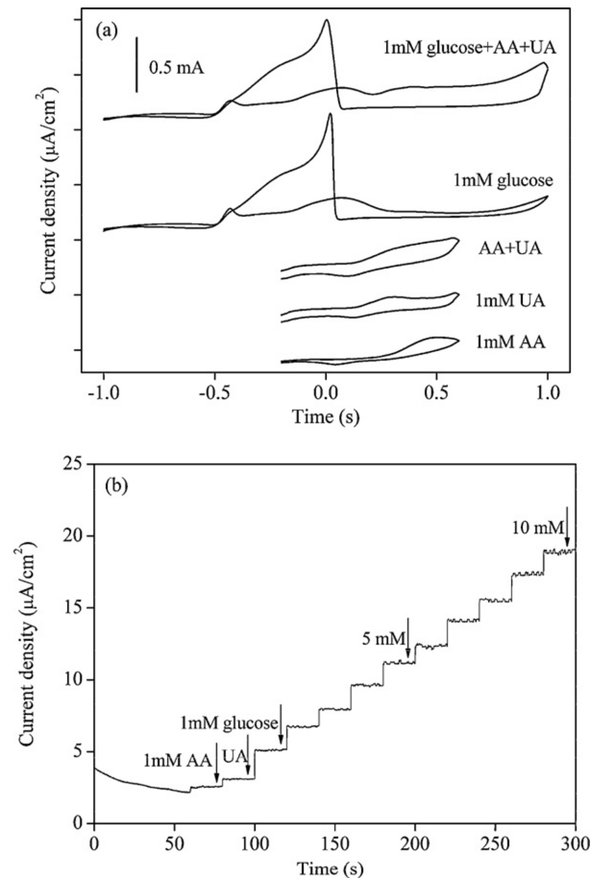

Fig. 7. (a) Cycle voltammograms of 1 mM AA, UA and their mixture without and with 1 mM glucose on the Au/DLC:P-0.1 electrode in the 0.1 M NaOH solution, and (b) current density–time response for glucose oxidation at the Au/DLC:P-0.1 electrodes with successive addition of glucose into the 0.1 M NaOH solution with 1 mM AA and UA at a potential of 0.1 V.

3.4. Selective detection of glucose in the presence of ascorbic acid, uric acid and acetaminophen

Considering the existent of ascorbic acid (AA) and uric acid (UA) in blood, which oxidize at a comparable potential to glucose and may interfere with the electrochemical detection of glucose using the glucose sensors, we investigate the glucose oxidation at Au/DLC:P-0.1 surface when the concentrations of AA and UA comparable to blood glucose levels. Fig. 7a shows cycle voltammograms of 1 mM AA, UA (over the levels present in human blood) and their mixture without and with 1 mM glucose on the Au/DLC:P-0.1 electrode in a 0.1 M NaOH solution, respectively. The oxidation peaks of AA and UA are at about 0.5 V and 0.30 V, respectively. A broad peak at 0.36 V is observed when AA and UA are mixed in the 0.1 M NaOH solution. The oxidation peaks of glucose are still visible when 1 mM glucose is added to the mixture of AA and UA. Therefore, the Au/DLC:P electrode may be good for blood glucose determination without obvious interference from AA and UA at least at a lower potential (<0.2 V). The current density–time response for glucose oxidation with successive addition of glucose into the 0.1 M NaOH solution with 1 mM AA and UA is also obtained at a potential of 0.1 V (Fig. 7b). The amperometric response of Au/DLC:P-0.1 to glucose additions in the presence of AA and UA is more evident, indicating that AA and UA have little interference on the glucose oxidation at Au/DLC:P surfaces.

4. Conclusion

Gold nanostructures with controllable hemispherical, branched and flower-like morphologies were electrochemically deposited on phosphorus doped diamond-like carbon (DLC:P) surfaces by solely controlling the deposition potential. The fitting of potentiostatic current–time transient with the Scharifker–Hills model showed a progressive nucleation of gold with diffusion-controlled on the DLC:P surface. The surface characters of flow-like gold nanostructures, such as large surface area, high oxidation degree and high-unsaturation (2 2 0) and (3 1 1) crystal faces might contribute the nanostructures with high catalytic activity for glucose electro-oxidation in alkaline media by the electrocatalysis model of hydrous oxide mediation of gold. The Au/DLC:P electrode showed a low electrochemical response to common interfering species including ascorbic acid and uric acid in blood, and therefore had little effect on glucose analysis at least at a low potential. The use of the DLC:P electrodes anchored with morphology-controllable gold nanostructures as an amperometric glucose sensor might solve the problem of intrinsically instability related to enzyme-based glucose sensors, thus would be promising for the development of a non-enzymatic glucose sensor.

Acknowledgments

This work is partly supported by the National Natural Science Foundation of China (Grant No. 50902123), the Visiting Scholars Fund of State Key Lab of Silicon Materials, Zhejiang University (Grant No. SKL2011-20), the Qianjiang Talent Program of Zhejiang Province (Grant No. QJD1102007), the National Basic Research Program of China (973 Program) (Grant No. 2010CB933501), the Excellent Young Talents Foundation of Key Laboratory of Advanced Textile Materials and Manufacturing Technology (Zhejiang Sci-Tech University) (Grant No. 2011QN05), and the Science Foundation of Zhejiang Sci-Tech University (Grant No. 0813824-Y).

References

[1] S.J. Updike, M.C. Shults, B.J. Gilligan, R.K. Rhodes, A subcutaneous glucose sensor with improved longevity, dynamic range, and stability of calibration, Diabetes Care 23 (2000) 208–214.
[2] S. Park, H. Boo, T.D. Chung, Electrochemical non-enzymatic glucose sensors, Anal. Chim. Acta 556 (2006) 46–57.
[3] K.E. Toghill, R.G. Compton, Electrochemical non-enzymatic glucose sensors: a perspective and an evaluation, Int. J. Electrochem. Sci. 5 (2010) 1246–1301.
[4] M.C. Daniel, D. Astruc, Gold nanoparticles: assembly, supramolecular chemistry, quantum-size-related properties, and applications toward biology, catalysis, and nanotechnology, Chem. Rev. 104 (2004) 293–346.
[5] X.G. Hu, S.J. Dong, Metal nanomaterials and carbon nanotubes – synthesis, functionalization and potential applications towards electrochemistry, J. Mater. Chem. 18 (2008) 1279–1295.
[6] B. Hvolbaek, T.V.W. Janssens, B.S. Clausen, H. Falsig, C.H. Christensen, J.K. Norskov, Catalytic activity of Au nanoparticles, Nano Today 2 (2007) 14–18.
[7] X.J. Bo, J. Bai, L. Yang, L.P. Guo, The nanocomposite of PtPd nanoparticles/onion-like mesoporous carbon vesicle for nonenzymatic amperometric sensing of glucose, Sens. Actuators B: Chem. 157 (2011) 662–668.
[8] K.E. Toghill, L. Xiao, M.A. Phillips, R.G. Compton, The non-enzymatic determination of glucose using an electrolytically fabricated nickel microparticle modified boron-doped diamond electrode or nickel foil electrode, Sens. Actuators B: Chem. 147 (2010) 642–652.
[9] P. Parpot, S.G. Pires, A.P. Bettencourt, Electrocatalytic oxidation of d-galactose in alkaline medium, J. Electroanal. Chem. 566 (2004) 401–408.
[10] Z.N. Liu, L.H. Huang, L.L. Zhang, H.Y. Ma, Y. Ding, Electrocatalytic oxidation of D-glucose at nanoporous Au and Au–Ag alloy electrodes in alkaline aqueous solutions, Electrochim. Acta 54 (2009) 7286–7293.
[11] J. Chen, J.H. Tang, F. Yan, H.X. Ju, A gold nanoparticles/sol–gel composite architecture for encapsulation of immunoconjugate for reagentless electrochemical immunoassay, Biomaterials 27 (2006) 2313–2321.
[12] Y.D. Jin, X.F. Kang, Y.H. Song, B.L. Zhang, G.J. Cheng, S.J. Dong, Controlled nucleation and growth of surface-confined gold nanoparticles on a (3-aminopropyl)trimethoxysilane-modified class slide: a strategy for SPR substrates, Anal. Chem. 73 (2001) 2843–2849.
[13] L. Cheng, A.P. Liu, S. Peng, H.W. Duan, Responsive plasmonic assemblies of amphiphilic nanocrystals at oil–water interfaces, ACS Nano 4 (2010) 6098–6104.
[14] Y.G. Sun, Y.N. Xia, Shape-controlled synthesis of gold and silver nanoparticles, Science 298 (2002) 2176–2179.
[15] S.S. Shankar, A. Ahmad, R. Pasricha, M. Sastry, Bioreduction of chloroaurate ions by geranium leaves and its endophytic fungus yields gold nanoparticles of different shapes, J. Mater. Chem. 13 (2003) 1822–1826.
[16] X.P. Sun, S.J. Dong, E. Wang, Large-scale synthesis of micrometer-scale single-crystalline Au plates of nanometer thickness by a wet-chemical route, Angew. Chem. Int. Ed. 43 (2004) 6360–6363.
[17] S.H. Chen, Z.L. Wang, J. Ballato, S.H. Foulger, D.L. Carroll, Monopod, bipod, tripod, and tetrapod gold nanocrystals, J. Am. Chem. Soc. 125 (2003) 16186–16187.
[18] J.E. Millstone, S. Park, K.L. Shuford, L.D. Qin, G.C. Schatz, C.A. Mirkin, Observation of a quadrupole plasmon mode for a colloidal solution of gold nanoprisms, J. Am. Chem. Soc. 127 (2005) 5312–5313.
[19] T.K. Sau, C.J. Murphy, Room temperature, high-yield synthesis of multiple shapes of gold nanoparticles in aqueous solution, J. Am. Chem. Soc. 126 (2004) 8648–8649.
[20] M. Grzelczak, J. Perez-Juste, P. Mulvaney, L.M. Liz-Marzan, Shape control in gold nanoparticle synthesis, Chem. Soc. Rev. 37 (2008) 1783–1791.
[21] A. Fukuoka, H. Araki, Y. Sakamoto, N. Sugimoto, H. Tsukada, Y. Kumai, Y. Akimoto, M. Ichikawa, Template synthesis of nanoparticle arrays of gold and platinum in mesoporous silica films, Nano Lett. 2 (2002) 793–795.
[22] Y. Li, G.Q. Shi, Electrochemical growth of two-dimensional gold nanostructures on a thin polypyrrole film modified ITO electrode, J. Phys. Chem. B 109 (2005) 23787–23793.
[23] X. Zhang, F. Shi, X. Yu, H. Liu, Y. Fu, Z.Q. Wang, L. Jiang, X.Y. Li, Polyelectrolyte multilayer as matrix for electrochemical deposition of gold clusters: toward super-hydrophobic surface, J. Am. Chem. Soc. 126 (2004) 3064–3065.
[24] P.N. Bartlett, J.J. Baumberg, P.R. Birkin, M.A. Ghanem, M.C. Netti, Highly ordered macroporous gold and platinum films formed by electrochemical deposition through templates assembled from submicron diameter monodisperse polystyrene spheres, Chem. Mater. 14 (2002) 2199–2208.
[25] A. Roucoux, J. Schulz, H. Patin, Reduced transition metal colloids: a novel family of reusable catalysts, Chem. Rev. 102 (2002) 3757–3778.
[26] J.S. Yu, T. Fujita, A. Inoue, T. Sakurai, M.W. Chen, Electrochemical synthesis of palladium nanostructures with controllable morphology, Nanotechnology 21 (2010) 085601–085608.
[27] S. Guo, L. Wang, E. Wang, Templateless, surfactantless, simple electrochemical route to rapid synthesis of diameter-controlled 3D flowerlike gold microstructure with “clean” surface, Chem. Commun. 30 (2007) 3163–3165.
[28] Y.H. Song, K. Cui, L. Wang, S.H. Chen, The electrodeposition of Ag nanoparticles on a type I collagen-modified glassy carbon electrode and their applications as a hydrogen peroxide sensor, Nanotechnology 20 (2009) 105501–105509.
[29] B.J. Plowman, S.K. Bhargava, A.P. O’Mullane, Electrochemical fabrication of metallic nanostructured electrodes for electroanalytical applications, Analyst 136 (2011) 5107–5119.
[30] S.Q. Liu, H.X. Ju, Reagentless glucose biosensor based on direct electron transfer of glucose oxidase immobilized on colloidal gold modified carbon paste electrode, Biosens. Bioelectron. 19 (2003) 177–183.
[31] R.L. McCreery, Advanced carbon electrode materials for molecular electrochemistry, Chem. Rev. 108 (2008) 2646–2687.
[32] D.D. La, C.K. Kim, T.S. Jun, Y.J. Jung, G.H. Seong, J. Choo, Y.S. Kim, Pt Nanoparticle-supported multiwall carbon nanotube electrodes for amperometric hydrogen detection, Sens. Actuators B: Chem. 155 (2011) 191–198.
[33] A.P. Liu, E.J. Liu, G.C. Yang, N.W. Khun, W.G. Ma, Non-enzymatic glucose detection using nitrogen-doped diamond-like carbon electrodes modified with gold nanoclusters, Pure Appl. Chem. 82 (2010) 2217–2229.
[34] D.B. Luo, L.Z. Wu, J.F. Zhi, Fabrication of Boron-doped diamond nanorod forest electrodes and their application in nonenzymatic amperometric glucose biosensing, ACS Nano 3 (2009) 2121–2128.
[35] Y. Liu, M.K. Wang, F. Zhao, Z.A. Xu, S.J. Dong, The direct electron transfer of glucose oxidase and glucose biosensor based on carbon nanotubes/chitosan matrix, Biosens. Bioelectron. 21 (2005) 984–988.
[36] J. Robertson, Diamond-like amorphous carbon, Mater. Sci. Eng. R: Rep. 37 (2002) 129–281.
[37] M. Benlahsen, H. Cachet, S. Charvet, C. Debiemme-Chouvy, C. Deslouis, A. Lagrini, V. Vivier, Improvement and characterization of the electrochemical reactivity of amorphous carbon nitride electrodes, Electrochem. Commun. 7 (2005) 496–499.
[38] A.P. Liu, W.J. Dong, E.J. Liu, W.H. Tang, J.Q. Zhu, J.C. Han, Non-enzymatic hydrogen peroxide detection using gold nanoclusters-modified phosphorus incorporated tetrahedral amorphous carbon electrodes, Electrochim. Acta 55 (2010) 1971–1977.
[39] A.P. Liu, J.Q. Zhu, J.C. Han, H.P. Wu, C.Z. Jiang, Fabrication and characterization of gold nanoclusters on phosphorus incorporated tetrahedral amorphous carbon electrode, Electrochem. Commun. 10 (2008) 827–830.
[40] B. Khadro, A. Sikora, A.-S. Loir, A. Errachid, F. Garrelie, C. Donnet, N. Jaffrezic-Renault, Electrochemical performances of B doped and undoped diamond-like carbon (DLC) films deposited by femtosecond pulsed laser ablation for heavy metal detection using square wave anodic stripping voltammetric (SWASV) technique, Sens. Actuators B: Chem. 155 (2011) 120–125.
[41] V. Rehacek, I. Hotovy, M. Vojs, Bismuth-coated diamond-like carbon microelectrodes for heavy metals determination, Sens. Actuators B: Chem. 127 (2007) 193–197.
[42] T. Kuroda, T. Irisawa, A. Ookawa, Growth of a polyhedra crystal from solution and its morphological stability, J. Cryst. Growth 42 (1977) 41–46.
[43] Y. Oaki, H. Imai, Experimental demonstration for the morphological evolution of crystals grown in gel media, Cryst. Growth Des. 3 (2003) 711–716.
[44] J.D. Hoefelmeyer, K. Niesz, G.A. Somorjai, T.D. Tilley, Radial anisotropic growth of rhodium nanoparticles, Nano Lett. 5 (2005) 435–438.
[45] JCPDS – International centre for diffraction data PCPDF win V 20.1, card no 01-1172, 1998.
[46] X.P. Sun, S.J. Dong, E.K. Wang, High-yield synthesis of large single-crystalline gold nanoplates through a polyamine process, Langmuir 21 (2005) 4710–4712.
[47] C. Hammond, The Basics of Crystallography and Diffraction, Oxford University Press, Oxford, 1997.

[48] L.D. Burke, J.M. Moran, P.F. Nugent, Cyclic voltammetry responses of metastable gold electrodes in aqueous media, J. Solid State Electrochem. 7 (2003) 529–538.
[49] M. Paunovic, M. Schlesinger, Fundamentals of Electrochemical Deposition, John Wiley and Sons, 1998.
[50] B. Scharifker, G. Hills, Theoretical and experimental studies of multiple nucleation, Electrochim. Acta 28 (1983) 879–889.
[51] F. Montilla, E. Morallon, I. Duo, C. Comninellis, J.L. Vazquez, Platinum particles deposited on synthetic boron-doped diamond surfaces application to methanol oxidation, Electrochim. Acta 48 (2003) 3891–3897.
[52] G.J. Lu, G. Zangari, Electrodeposition of platinum on highly oriented pyrolytic graphite. Part 1: electrochemical characterization, J. Phys. Chem. B 109 (2005) 7998–8007.
[53] L.D. Burke, T.G. Ryan, The role of incipient hydrous oxides in the oxidation of glucose and some of its derivatives in aqueous media, Electrochim. Acta 37 (1992) 1363–1370.
[54] L.D. Burke, W.A. O'Leary, Mediation of oxidation reactions at noble metal anodes by low levels of in situ generated hydroxy species, J. Electrochem. Soc. 135 (1988) 1664–1965.
[55] G.A. Somorjai, Introduction to Surface Chemistry and Catalysis, Wiley, 1994.
[56] B.J. Plowman, A.P. O'Mullane, P.R. Selvakannan, S.K. Bhargava, Honeycomb nanogold networks with highly active sites, Chem. Commun. 46 (2010) 9182–9184.

Biographies

Aiping Liu, Dr. Degree, obtained from Harbin Institute of Technology, China in July 2008. Dr. Liu is employed by Center for Optoelectronics Materials and Devices in Zhejiang Sci-Tech University of China as an associate professor and a visiting researcher in State Key Lab of Silicon Materials in Zhejiang University of China. Current fields of interest of Dr. Liu are focused on metal-modified carbon-based nanomaterials and their application in electrochemical sensor or biosensor.

Qinghua Ren is currently a candidate for Master degree in the Zhejiang Sci-Tech University, China. Her Master research focuses on nanocomposite carbon material and its application in sensor.

Tao Xu is pursuing his Master degree in the Zhejiang Sci-Tech University, China. His Master work focuses on the application of diamond-like carbon films as biosensors and electrochemical sensors.

Ming Yuan is a master course student in the Zhejiang Sci-Tech University, China. His research interests are the synthesis and characteristic of nanosized materials.

Weihua Tang is a professor in the Beijing University Posts and Telecommunications, China. His research includes thin films and coatings, and nanomaterials for optoelectronics devices and microfabrication technology.